Lu, C., Li, X., Li, Z., Heinkelmann, R., Nilsson, T., Dick, G., Ge, M., Schuh, H. (2016): GNSS tropospheric gradients with high temporal resolution and their effect on precise positioning. - *Journal of Geophysical Research, 121*, 2, pp. 912—930.

DOI: http://doi.org/10.1002/2015JD024255

AGU PUBLICATIONS

JGR

Journal of Geophysical Research: Atmospheres

RESEARCH ARTICLE
10.1002/2015JD024255

Key Points:
- The rapid development of multi-GNSS has potential to provide high-resolution tropospheric gradients
- We develop a multi-GNSS process for the precise retrieval of high-resolution tropospheric gradients
- The benefits of multi-GNSS for tropospheric gradients and precise positioning are demonstrated

Correspondence to:
X. Li,
lixin@gfz-potsdam.de

Citation:
Lu, C., X. Li, Z. Li, R. Heinkelmann, T. Nilsson, G. Dick, M. Ge, and H. Schuh (2016), GNSS tropospheric gradients with high temporal resolution and their effect on precise positioning, *J. Geophys. Res. Atmos.*, *121*, 912–930, doi:10.1002/2015JD024255.

Received 21 SEP 2015
Accepted 28 DEC 2015
Accepted article online 4 JAN 2016
Published online 29 JAN 2016

GNSS tropospheric gradients with high temporal resolution and their effect on precise positioning

Cuixian Lu[1], Xingxing Li[1], Zhenhong Li[2], Robert Heinkelmann[1], Tobias Nilsson[1], Galina Dick[1], Maorong Ge[1], and Harald Schuh[1]

[1]German Research Centre for Geosciences GFZ, Potsdam, Germany, [2]COMET, School of Civil Engineering and Geosciences, Newcastle University, Newcastle upon Tyne, UK

Abstract The tropospheric horizontal gradients with high spatiotemporal resolutions provide important information to describe the azimuthally asymmetric delays and significantly increase the ability of ground-based GNSS (Global Navigation Satellite Systems) within the field of meteorological studies, like the nowcasting of severe rainfall events. The recent rapid development of multi-GNSS constellations has potential to provide such high-resolution gradients with a significant degree of accuracy. In this study, we develop a multi-GNSS process for the precise retrieval of high-resolution tropospheric gradients. The tropospheric gradients with different temporal resolutions, retrieved from both single-system and multi-GNSS solutions, are validated using independent numerical weather models (NWM) data and water vapor radiometer (WVR) observations. The benefits of multi-GNSS processing for the retrieval of tropospheric gradients, as well as for the improvement of precise positioning, are demonstrated. The multi-GNSS high-resolution gradients agree well with those derived from the NWM and WVR, especially for the fast-changing peaks, which are mostly associated with synoptic fronts. The multi-GNSS gradients behave in a much more stable manner than the single-system estimates, especially in cases of high temporal resolution, benefiting from the increased number of observed satellites and improved observation geometry. The high-resolution multi-GNSS gradients show higher correlation with the NWM and WVR gradients than the low-resolution gradients. Furthermore, the precision of station positions can also be noticeably improved by multi-GNSS fusion, and enhanced results can be achieved if the high-resolution gradient estimation is performed, instead of the commonly used daily gradient estimation in the multi-GNSS data processing.

1. Introduction

The application of ground-based GPS receivers to the sounding of atmospheric water vapor was introduced in the early 1990s [*Bevis et al*., 1992; *Duan et al*., 1996; *Rocken et al*., 1997], and remarkable progress in the field of atmospheric remote sensing using GPS has been achieved in the last decades [*Fang et al*., 1998; *Li et al*., 2003; *Gendt et al*., 2004; *Li et al*., 2014, 2015a]. Its low cost, high spatiotemporal resolution, all-weather availability, and high accuracy make ground-based GPS a uniquely powerful water vapor observing system [*Bar-Sever et al*., 1998]. As the basis of GPS meteorology, the estimated tropospheric parameter, commonly referred to as zenith total delay (ZTD), can be converted into precipitable water vapor (PWV) using surface pressure and temperature measurements [*Bevis et al*., 1994]. Nowadays, the ZTD derived from GPS is widely used to be assimilated into numerical weather models (NWM), to both improve weather forecasts and monitor climate change [e.g., *Gradinarsky et al*., 2002; *Gendt et al*., 2004; *Poli et al*., 2007; *Nilsson and Elgered*, 2008]. The operational usage of GPS ZTD for meteorological application at several weather agencies worldwide [e.g., *Poli et al*., 2007] and the establishment of several related European projects—such as WAVEFRONT, MAGIC, COST-716 [*Elgered et al*., 2005], E-GVAP, and European Earth System Science and Environmental Management (ESSEM) COST Action ES1206 (GNSS4SWEC)—demonstrate the ability of GPS as an accurate water vapor sensor for meteorological applications and the benefit of GPS-derived ZTD for short-term severe weather forecasts [*Karabatic et al*., 2011; *Dousa and Vaclavovic*, 2014].

However, the spatiotemporal distribution of atmospheric water vapor is highly variable and cannot be adequately modeled by a mapping function assuming symmetry of the water vapor distribution in all azimuth directions. Ignoring the azimuthal asymmetry of the neutral atmosphere may result in a negative influence on such high-precision GNSS (Global Navigation Satellite Systems) applications as long-term geodynamics

studies, the realization of territorial reference frames, and meteorological and climatological interpretations [*Ghoddousi-Fard et al*., 2009]. The ZTD provides only vertically integrated information on the atmospheric refractivity, whereas the information in connection with horizontal atmospheric distribution is not considered. To account for the horizontal anisotropy of refractivity in the troposphere, atmospheric gradients were introduced [e.g., *MacMillan*, 1995]. This anisotropy occurs most significantly in the vicinity of strong horizontal humidity gradients, such as frontal regions, which in turn are associated with severe weather phenomena [*Miyazaki et al*., 2003]. The acquisition of enhanced meteorological information content can thus benefit from the accurate sensing of tropospheric gradients.

The tropospheric delay gradient model [e.g., *MacMillan*, 1995; *Chen and Herring*, 1997] expresses the tropospheric delay as a sum of ZTD and horizontal gradients. The first implementation of a tropospheric gradient model into GPS data analysis was carried out by *Bar-Sever et al*. [1998]. They demonstrated that the gradient model improved the station position repeatability of GPS precise point positioning (PPP) [*Zumberge et al*., 1997] in most cases. Improvements in the precision of station position estimates from the perspective of both point positioning and network solutions, obtained by taking into account inhomogeneities in the atmospheric water vapor distribution above GPS stations, were also demonstrated by many other previous studies [e.g., *Miyazaki et al*., 2003; *Meindl et al*., 2004]. *Iwabuchi et al*. [2003] pointed out that the tropospheric delay gradient model could also improve the accuracy of ZTD estimates. The estimation of tropospheric horizontal gradients together with zenith delays is now a commonly adopted technique carried out by a wide range of GPS processing software programs [*Li et al*., 2015b]. For most IGS (International GNSS Service) analysis centers (e.g., Center for Orbit Determination in Europe, European Space Agency, Deutsches GeoForschungsZentrum, and Massachusetts Institute of Technology), a pair of horizontal gradient parameters representing north and east directions of each GNSS station is estimated in an interval of 24 h. The piecewise gradient parameters are usually estimated on a daily basis to avoid large variations and jumps in the gradients and to reduce the number of parameters estimated epoch-wise [*Meindl et al*., 2004]. However, as stressed by the results obtained from NWM, tropospheric gradients may vary by several millimeters over a time period much shorter than 24 h. Furthermore, since it is the tropospheric gradient rather than the PWV that is highly correlated with strong rainfall events, high-resolution gradient parameters are desired in terms of contributing to severe rainfall nowcasting [*Shoji*, 2013].

With the modernization of GPS, recovery of Global Navigation Satellite System (GLONASS), and newly emerging constellations (e.g., BeiDou and Galileo), the global satellite navigation has experienced dramatic changes within the field of multi-constellation GNSS [*Montenbruck et al*., 2014; *Li et al*., 2015c]. For example, the Galileo system is working towards a fully operational campaign, with currently eight satellites deployed in orbit. The Chinese BeiDou system officially launched a regional navigation service at the end of 2012, which will continue to develop to a global system in the near future. Additionally, the Japanese Quasi-Zenith Satellite System (QZSS) and the Indian Regional Navigation Satellite System (IRNSS) have both launched their first satellites. Currently, more than 80 navigation satellites from different navigation systems (32 GPS, 24 GLONASS, 17 BeiDou, 8 Galileo, 1 QZSS, and 1 IRNSS) are in orbit, and more than 120 satellites will be available once all systems are fully operational. On the basis of the changing world of GNSS, a multi-GNSS observation network, the MGEX (Multi-GNSS Experiment) network, with global coverage was established by IGS in 2012 to facilitate early experimentation and familiarization with the newly emerging signals and systems as well as to prepare a well-featured multi-GNSS service to the scientific community [*Montenbruck et al*., 2014]. Currently, more than 120 stations are included in the MGEX network, offering an excellent capability of multi-GNSS constellation tracking and delivering data which are of great interest and potential to both geodetic and geophysical applications [*Li et al*., 2015a, 2015b].

Compared to the single-system constellation (e.g., GPS), where the accuracy of high-resolution gradient estimates is limited by the observing geometry due to insufficient number of satellites in view and inhomogeneous geometric coverage of available satellites, it is expected that high-resolution gradients with enhanced accuracy and stability can be provided by the multi-GNSS processing, with more satellites and improved spatial geometry. As demonstrated by *Li et al*. [2015d], the high-resolution multi-GNSS (a combination of four systems: GPS, GLONASS, Galileo, and BeiDou) gradients agreed quite well with those derived from a water vapor radiometer (WVR). These initial results related to multi-GNSS tropospheric gradients are promising but further studies concerning the performance of the gradients estimated with different temporal resolutions, retrieved from

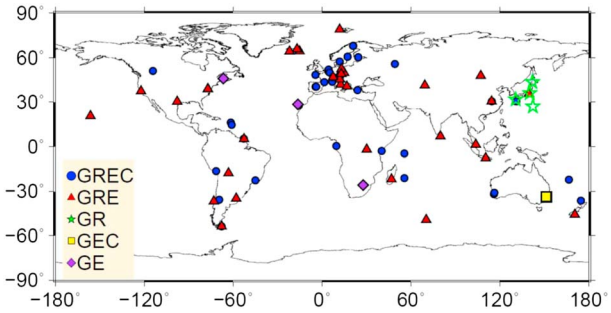

Figure 1. Distribution of MGEX stations and their supported constellations. The symbols G, R, E, and C represent GPS, GLONASS, Galileo and BeiDou, respectively.

each single GNSS, as well as from the combined multi-GNSS solution, are still required, particularly in relation to their effects on precise positioning.

In this contribution, we develop a multi-GNSS processing system designed for high-resolution tropospheric gradient estimation based on the PPP technique. Observations taken from the stations of the IGS MGEX network are processed, and high-resolution tropospheric gradients from both single-system (GPS, GLONASS, and BeiDou) and multi-GNSS (a combination of GPS, GLONASS, Galileo, and BeiDou) solutions are retrieved. The performance of tropospheric gradients estimated with different temporal resolutions derived from single-system and multi-GNSS solutions is assessed and validated by comparing the results with NWM and WVR data. Furthermore, the effects of high-resolution gradient estimation on precise positioning in both static and kinematic modes are investigated. The benefits of multi-GNSS processing for gradient derivation, as well as for the improvement of precise positioning, are demonstrated.

This article is organized as follows. We first describe the data collection, including the GNSS data, NWM, and WVR gradient data in section 2, where the GNSS gradient estimation strategies are also presented. In section 3, the performance of GNSS tropospheric gradients estimated with different temporal resolutions and retrieved from different systems is evaluated in detail, alongside with comparisons and validations of NWM and WVR gradients. Additionally, the effects of tropospheric gradient estimation with different temporal resolutions on the repeatability of station coordinates for static positioning and on the precision of kinematic positioning are analyzed in section 4. The conclusions are summarized in section 5.

2. Data Collection and Processing

2.1. GNSS Data Collection

The MGEX campaign (http://igs.org/mgex/) was initialized by the IGS to track, collect, and analyze all available signals from GPS, GLONASS, BeiDou, Galileo, QZSS, and any other space-based augmentation system of interest. Under the framework of the MGEX project, a new worldwide network of multi-GNSS monitoring stations has been established over the past 2 years in parallel with the IGS network, which is only served for GPS and GLONASS. Today, the MGEX network comprises more than 120 globally distributed stations, providing excellent capabilities of multi-GNSS constellation tracking, which benefits hugely from contributions from around 27 agencies, universities, and other institutions from 16 countries (http://igs.org/mgex). In addition to the tracking of GPS constellation, each MGEX station can track at least one of the new BeiDou, Galileo, or QZSS constellations. Furthermore, GLONASS observations are available from the majority of the MGEX stations. Currently, around 80 reference stations are capable of tracking the GLONASS satellites, 75 stations are tracking the Galileo satellites, whereas the BeiDou constellation is tracked by more than 30 receivers. The geographic distribution of the MGEX stations and their supported constellations are shown in Figure 1.

2.2. NWM and WVR Data Collection

The NWM use a large variety of meteorological observations to describe atmospheric dynamics and compute weather forecasts. Unlike the existing observation systems, no new observations are generated from a NWM. Instead, the NWM assimilates a large number of different meteorological observations into a prediction based on the model background provided by atmosphere physics. One of the advantages of the global NWM is its capability of retrieving ZTD and horizontal gradients at any location. When applying a ray-trace algorithm [e.g., *Zus et al.*, 2014], the tropospheric delays on a site can be computed with high speed and precision for any given elevation and azimuth angles. For the acquisition of NWM-based tropospheric gradients in this study, pressure, temperature, and humidity fields available every 6 h (00:00, 06:00, 12:00, and 18:00 UTC) from the ECMWF (European Centre for Medium-Range Weather Forecasts) analysis (http://www.ecmwf.int/) are utilized. The ECMWF data are provided with a horizontal resolution of 1° × 1° on 137 vertical model levels extending

from the Earth's surface to about 80 km. To derive the tropospheric gradients at a particular location from ECMWF data using the ray-trace algorithm, several steps are needed. First, a set of azimuth-dependent tropospheric delays are calculated, with the spacing in azimuth being 30° and the elevation angles being 3°, 5°, 7°, 10°, 15°, 20°, 30°, 50°, 70°, and 90°. Second, a set of azimuth-independent tropospheric delays are computed, assuming that the atmosphere is spherically layered. Then, the corresponding differences between the azimuth-dependent and azimuth-independent tropospheric delays are calculated. Finally, the tropospheric gradients are retrieved using a least squares fit to the computed residuals in the last step and the gradient mapping function from *Chen and Herring* [1997]. Although the sampling rate of gradient estimates from GNSS is higher than that from the ECMWF, no temporal interpolation is applied during the comparison to avoid introducing additional errors. Only gradient estimates at the common epochs of both techniques are considered for the comparison.

The WVR operated at the Onsala Space Observatory is co-located with the multi-GNSS station ONS1, with a distance of about 10 m and a height difference of less than 1 m. The WVR measures the thermal sky emission, which is caused by the water vapor, the liquid water, and the oxygen in the atmosphere, at the two frequencies 21.0 and 31.4 GHz. The WVR is operated continuously in a "sky-mapping" mode, which corresponds to a repeated cycle of 60 observations spread over the sky with elevation angles of no less than 20°; typically, this results in 6000–9000 measurements per day. The wet delays from the WVR are inferred from the sky brightness temperatures [*Elgered and Jarlemark*, 1998]. The formal uncertainty of wet delay estimates varies with the elevation angle and weather conditions, usually ranging from 0.5 mm to 3.0 mm. However, the absolute uncertainty (magnitude of 1 standard deviation) is on the order of about 7 mm, when an uncertainty of 1 K is assumed for the observed sky brightness temperature. The gradient estimates are not directly provided by the WVR; rather, they are estimated along with the zenith delays by using all the acquired line-of-sight observations to an in-house software package, applying the model presented in equation (3). The estimation process is similar to that implemented in the GNSS processing, and the gradients are solved by a least squares estimator for different time resolutions, e.g., 15 min, 1 h, or 2 h (here 1 h resolution is used). The gradients retrieved from WVR provide a direct assessment of the performance of the GNSS-based estimates. However, it is noteworthy that the WVR data only provide wet gradients, while GNSS data produce total gradients which include both wet and dry elements. For further comparison and validation with the GNSS-based estimates, WVR wet gradients are corrected with the ECMWF dry gradients to derive the total gradients [*Li et al*., 2015d]. The 6 h dry gradients of ECMWF are linearly interpolated to be consistent with the WVR wet gradients of 1 h interval. The corrected gradient values, which contain not only the wet component but also the dry component, are referred to as the total WVR gradient and are used in this study.

2.3. GNSS Gradient Estimation

In the PPP processing, precise satellite orbits and clocks are fixed to previously determined values. The PPP model for multi-GNSS processing (here GPS, GLONASS, Galileo, and BeiDou) can be formulated as

$$\begin{cases} l_{r,j}^{G} = -\mathbf{u}_r^{G}\cdot\mathbf{r}_r + t_r + \lambda_{jG}\left(b_{rG,j} - b_j^{\,G}\right) + \lambda_{jG}N_{r,j}^{G} - \kappa_{jG}\cdot I_{r,1}^{G} + T_r + \varepsilon_{r,j}^{G} \\ l_{r,j}^{R_k} = -\mathbf{u}_r^{R}\cdot\mathbf{r} + t_r + \lambda_{jR_k}\left(b_{rR_k,j} - b_j^{\,R}\right) + \lambda_{jR_k}N_{r,j}^{R} - \kappa_{jR_k}\cdot I_{r,1}^{R} + T_r + \varepsilon_{r,j}^{R} \\ l_{r,j}^{E} = -\mathbf{u}_r^{E}\cdot\mathbf{r} + t_r + \lambda_{jE}\left(b_{rE,j} - b_j^{\,E}\right) + \lambda_{jE}N_{r,j}^{E} - \kappa_{jE}\cdot I_{r,1}^{E} + T_r + \varepsilon_{r,j}^{E} \\ l_{r,j}^{C} = -\mathbf{u}_r^{C}\cdot\mathbf{r}_r + t_r + \lambda_{jC}\left(b_{rC,j} - b_j^{\,C}\right) + \lambda_{jC}N_{r,j}^{C} - \kappa_{jC}\cdot I_{r,1}^{C} + T_r + \varepsilon_{r,j}^{C} \end{cases} \tag{1}$$

$$\begin{cases} p_{r,j}^{G} = -\mathbf{u}_r^{G}\cdot\mathbf{r}_r + t_r + c\cdot d_{rG} + \kappa_{jG}\cdot I_{r,1}^{G} + T_r + e_{r,j}^{G} \\ p_{r,j}^{R_k} = -\mathbf{u}_r^{R}\cdot\mathbf{r}_r + t_r + c\cdot d_{rR_k} + \kappa_{jR_k}\cdot I_{r,1}^{R} + T_r + e_{r,j}^{R} \\ p_{r,j}^{E} = -\mathbf{u}_r^{E}\cdot\mathbf{r}_r + t_r + c\cdot d_{rE} + \kappa_{jE}\cdot I_{r,1}^{E} + T_r + e_{r,j}^{E} \\ p_{r,j}^{C} = -\mathbf{u}_r^{C}\cdot\mathbf{r}_r + t_r + c\cdot d_{rC} + \kappa_{jC}\cdot I_{r,1}^{C} + T_r + e_{r,j}^{C} \end{cases} \tag{2}$$

where $l_{r,j}^{s}$ and $p_{r,j}^{s}$ denote the "observed minus computed" phase and pseudorange observables; r and j refer to receiver and frequency, respectively; The indices G, R, E, and C refer to the GPS, GLONASS, Galileo, and BeiDou satellites, respectively; R_k denotes the GLONASS satellite with frequency factor k; $\mathbf{u}_r^{s}$ is the unit vector of the direction from receiver to satellite; $\mathbf{r}_r$ denotes the vector of the receiver position increments relative to the a priori position which is used for linearization; t_r is the receiver clock bias; $N_{r,j}^{s}$ is the integer ambiguity; $b_{r,j}$, $b_j^{\,s}$ are the uncalibrated phase delays; λ_j is the wavelength; the ionospheric delays $I_{r,j}^{s}$ at different frequencies can

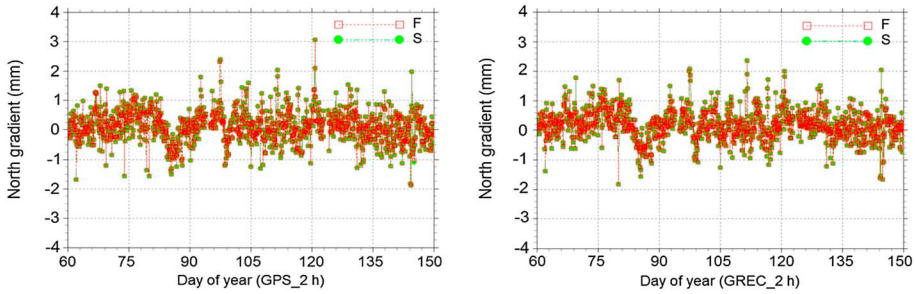

Figure 2. The north gradients retrieved every 2 h from GPS and multi-GNSS ("GREC") solution in PPP mode with the station positions being fixed ("F"), and estimated as static ("S") at multi-GNSS station ONS1 for day of year (DOY) 60–150 of 2014.

be expressed as $I^s_{r,j} = \kappa_j \cdot I^s_{r,1},\ \kappa_j = \lambda_j^2/\lambda_1^2$; and T_r is the slant tropospheric delay. Due to the different frequencies and signal structures of each individual GNSS, the code biases d_{rG}, d_{rR_k}, d_{rE}, and d_{rC} are different in each multi-GNSS receiver. These inter-system biases, and inter-frequency biases of the GLONASS satellites with different frequency factors, must be estimated or corrected in a combined processing of multi-GNSS observations. Parameters $e^s_{r,j}$ and $\varepsilon^s_{r,j}$ denote the sum of measurement noise and multipath for pseudorange and phase observations, respectively. The phase center offsets and variations, tidal loading, and phase wind-up can be corrected according to the existing models [*Kouba*, 2009].

To acquire information on the effects of the treatment of station positions, i.e., fixed or estimated as static, on the tropospheric gradient derivation, we calculate and compare the gradients derived from the two strategies. As an example, Figure 2 shows the north gradients retrieved every 2 h from GPS-only and the multi-GNSS solutions in PPP mode with the station positions being fixed and estimated as static at the multi-GNSS station ONS1 (Onsala, Sweden). The results show that regardless of whether the station positions are fixed or estimated as static, the gradient estimates remain unaffected. In order to avoid possible errors introduced by fixed station coordinates, in the following investigations, we estimate the station positions as static together with the other parameters.

To account for both homogeneity and inhomogeneity of the troposphere, the complete model for the slant tropospheric delay T can be expressed via gradient mapping function proposed by *Chen and Herring* [1997],

$$T = \mathrm{mf}_h \cdot \mathrm{ZHD} + \mathrm{mf}_{\mathrm{nh}} \cdot \mathrm{ZWD} + \mathrm{mf}_G \cdot (G_{\mathrm{ns}} \cdot \cos(a) + G_{\mathrm{ew}} \cdot \sin(a)) \tag{3}$$

where ZHD denotes zenith hydrostatic delay, which can be calculated with sufficient accuracy using empirical models such as the *Saastamoinen* [1973] model and in situ meteorological information. ZWD represents zenith wet delay and is estimated as parameters along with the north-south and east-west horizontal gradients, G_{ns} and G_{ew}, and other parameters in the PPP processing. Parameters mf_h and $\mathrm{mf}_{\mathrm{nh}}$ are the hydrostatic and nonhydrostatic mapping functions, respectively (here we use the Global Mapping Functions, [*Böhm et al*., 2006]), and mf_G is the gradient mapping function. Parameter a denotes the azimuth angle for the line of sight of the individual observation.

For the static multi-GNSS PPP processing, the estimated parameters vector $\mathbf{X}$ can be described as

$$\mathbf{X} = \left(\mathbf{r}_r\ t_r\ \mathrm{ZWD}\ G_{\mathrm{ns}}\ G_{\mathrm{ew}}\ d_{rE}\ d_{rC}\ d_{rR_k}\ \mathbf{I}^s_{r,1}\ \mathbf{N}^s_{r,j}\right)^T \tag{4}$$

observations from all four individual GNSS are processed together in one weighted least squares estimator in order to conduct a rigorous multi-GNSS analysis including estimation of the inter-system and inter-frequency biases. The receiver position increments are estimated as static parameters on a daily basis. The receiver clock bias t_r is estimated as white noise, and the inter-system and inter-frequency code biases are estimated as parameters on a daily basis. To eliminate the singularity between receiver clock and code bias parameters, the code biases for GPS satellites are set to zero. All the estimated biases for the other systems are relative to those for the GPS satellites. The phase delays b_j will be absorbed by phase ambiguity parameters $\mathbf{N}^s_r$, which are estimated as constants for each continuous arc. The ionospheric delays $\mathbf{I}^s_{r,1}$ are taken as estimated parameters for each satellite-site pair and each epoch by using the dual-frequency raw phase and pseudorange observations. The tropospheric zenith wet delay (ZWD) and the associated north and east horizontal gradients, G_{ns} and G_{ew}, are modeled as piecewise constant parameters with different time resolutions

(1 h, 2 h, 4 h, 6 h, and 12 h) for the derivation of gradient estimates with different temporal resolution. For the estimation of high-resolution horizontal gradients, a very loose relative constraint of about 30 mm/$\sqrt{\text{hour}}$ is imposed to track the fast-changing variation. A cutoff elevation angle of 7° is applied, and the elevation-dependent weighting strategy is also performed.

3. GNSS Gradients in High Temporal Resolution

3.1. Validation With ECMWF Gradients

To make an assessment on the tropospheric gradients estimated from individual GNSS: GPS, GLONASS, or BeiDou, and the combined four-system (i.e., GPS, GLONASS, BeiDou, and Galileo) solution, referred to as multi-GNSS solution, observations from the MGEX network are processed in PPP mode following the procedure described in section 2.3. The gradients derived with different navigation systems as well as with different temporal resolutions (1 h, 2 h, 4 h, 6 h, and 12 h) are carefully analyzed. Comparisons with ECMWF-derived gradients are performed as an external validation.

Taking MGEX station ONS1 (Sweden, 57.40°N, 11.93°E) as an example, the tropospheric horizontal gradients estimated with different temporal resolutions over a period of three months (March, April, and May) in 2014 are shown in Figure 3, where the gradients derived from ECMWF at the station positions at 6 h intervals are also displayed. In Figure 3a, GPS north gradients estimated with temporal resolutions of 1 h, 2 h, and 4 h are shown in Figure 3 (left column), while those estimated every 6 h and 12 h are shown in Figure 3 (right column). One can see that the 1 h GPS gradients show the largest deviations with respect to those of the ECMWF. Although the spike-shaped peaks, which are mostly associated with synoptic fronts, can be observed, the 1 h gradients tend to be the noisiest. The noise may be caused by the relative larger instability due to the decrease of the parameter interval length and the associated limitation of observational geometry.

The 6 h and 12 h GPS gradients agree better with those of the ECMWF, exhibiting fewer outliers and less noise. However, some spike-shaped peaks are not captured. This is because that the gradients from the weather model are a snapshot of the troposphere at a certain epoch, whereas the gradients from the GNSS techniques are averaged over a particular period. Such an averaging process will smooth the high-frequency variations of the gradients. The best agreement with the ECMWF gradients can be noted for those GPS gradients estimated with 2 h and 4 h time intervals, especially for the spike-shaped peaks, which are associated with the synoptic fronts. For this temporal resolution, obviously a trade-off between the temporal resolution and the robustness of the estimated gradients is achieved. Similar results can be found for the GLONASS gradients (Figure 3b) that are slightly noisier than GPS gradients in general.

It can be seen from Figure 3c that the gradients derived from BeiDou display significant differences with respect to ECMWF gradients for all estimation time resolutions. This may indicate that the tropospheric horizontal gradients estimated with the currently incomplete BeiDou constellation are not competitive with those derived from GPS or GLONASS. We expect the limited orbit geometry and/or the error models of BeiDou being a main cause of this effect but it needs to be explicitly verified in detail in future studies. Therefore, for the present study, BeiDou-only gradients will not be discussed furthermore. The Galileo-only gradients are not analyzed, as too few (eight currently) satellites are in orbit and the system cannot provide an autonomous application. The multi-GNSS gradients are presented in Figure 3d and the enlarged view of a gradient peak during the period of day of year (DOY) 75–105 are displayed in Figure 3e. When compared to the gradients estimated with other time resolutions, the 2 h multi-GNSS gradients present the best agreement with the ECMWF gradients and can well capture the peaks. Since the east gradients exhibit similar behaviors to the north gradients, they are not shown here.

Figure 4 compares the tropospheric gradients derived from GPS, GLONASS, and the multi-GNSS solutions at station ONS1 for the same period. The ECMWF gradients are depicted in blue lines for reference. Figures 4a–4e differ in terms of temporal resolution: 1 h, 2 h, 4 h, 6 h, and 12 h, respectively. It can be seen from Figure 4 that the GLONASS gradients indicate comparable accuracy to GPS gradients but exhibit slightly more noise and outliers. The gradients derived from the single-system solutions, both GPS and GLONASS, show more noise and outliers compared to the multi-GNSS solution, which may be caused by the lower number of observed GPS or GLONASS satellites and poor observation geometry under the single-system condition. The multi-GNSS gradients behave in a substantially more stable manner than the single-system estimates, especially in cases of

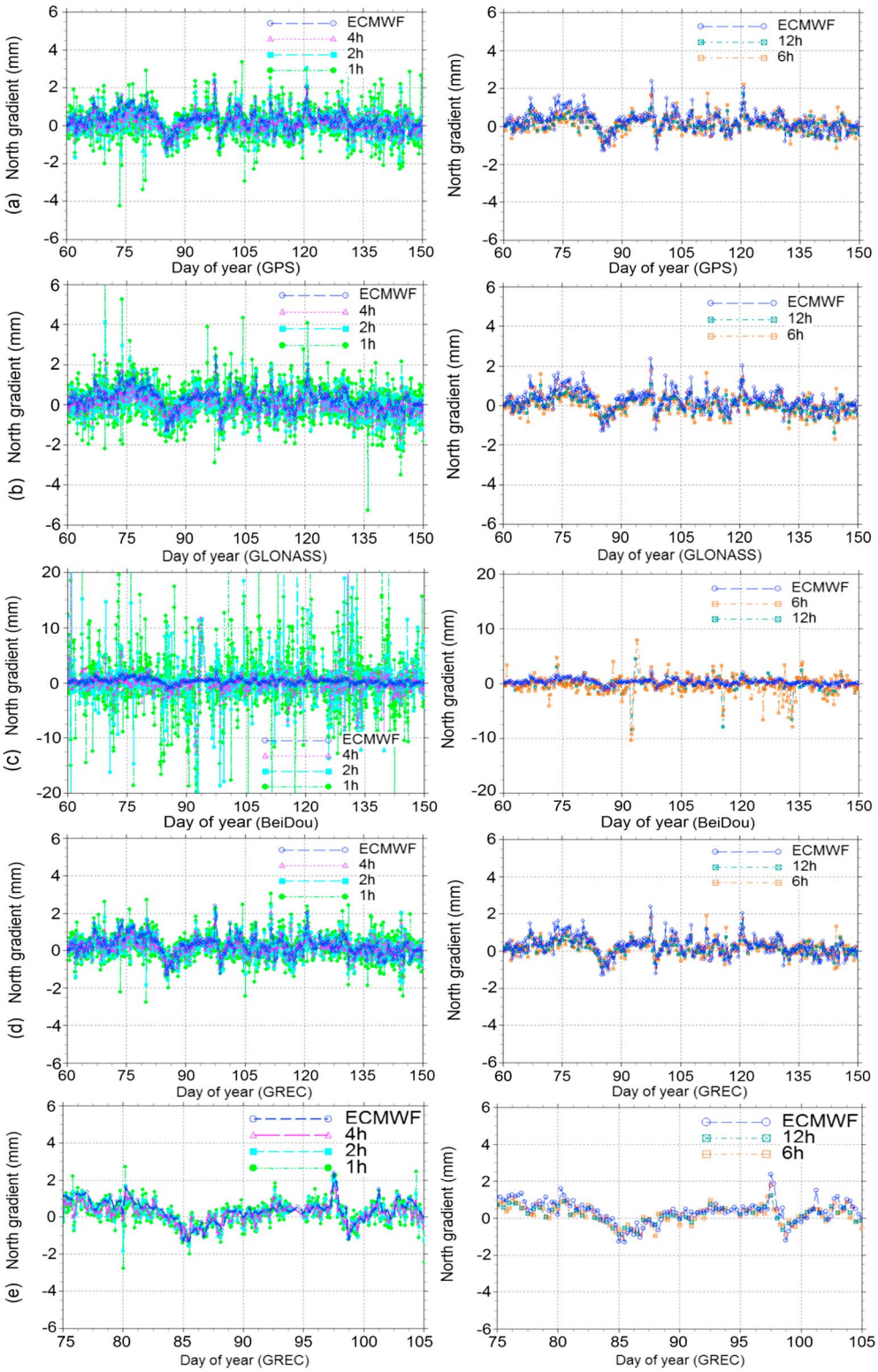

Figure 3. The north gradients estimated with different temporal resolutions at station ONS1 for DOY 60–150 of 2014. The (a) GPS, (b) GLONASS, (c) BeiDou, and (d) multi-GNSS gradients. (e) The enlarged view of a gradient peak for multi-GNSS solution during the period DOY 75–105. The gradients of 1 h, 2 h, and 4 h are shown in the left plot, while those estimated every 6 h and 12 h are shown in the right plot. The blue lines depict the tropospheric gradients derived from ECMWF.

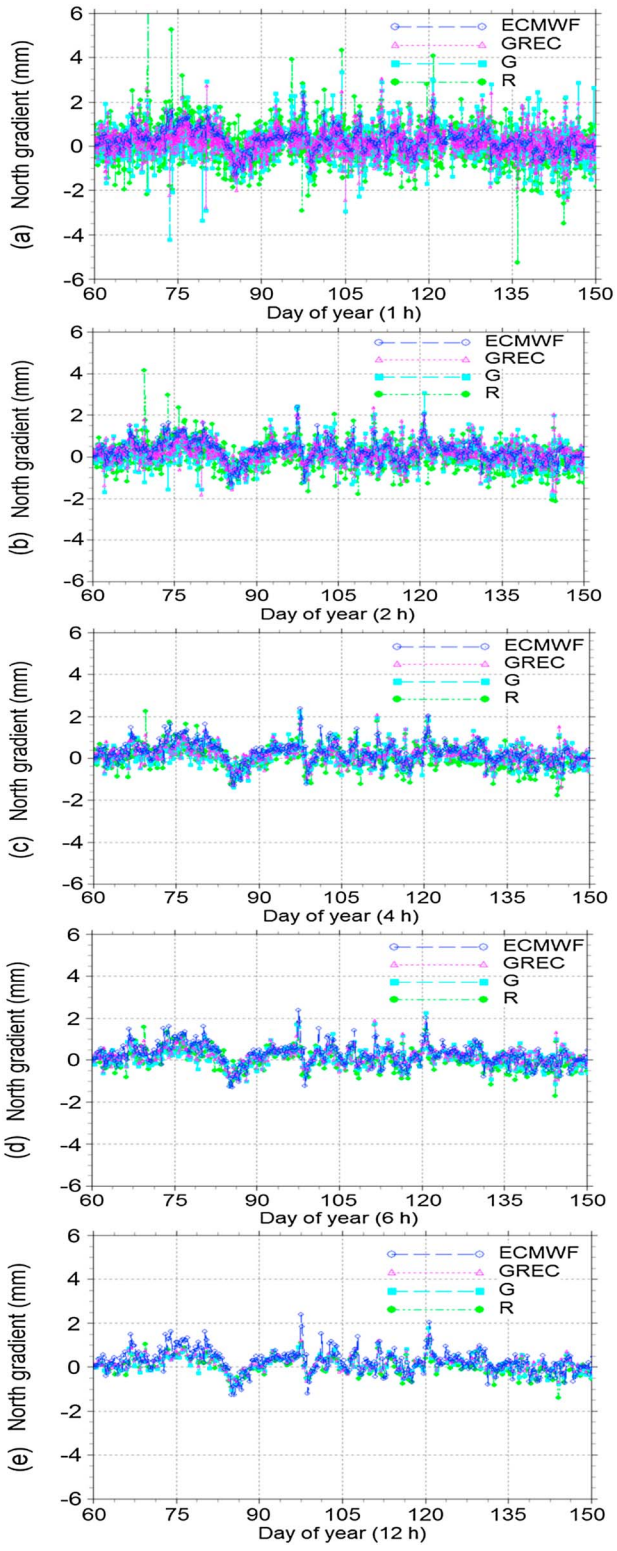

Figure 4. The north gradients derived from GPS ("G"), GLONASS ("R"), and multi-GNSS solutions at station ONS1 for DOY 60–150 of 2014. (a–e) The gradients estimated with the temporal resolutions of 1 h, 2 h, 4 h, 6 h, and 12 h are illustrated. The blue lines indicate the tropospheric gradients derived from ECMWF.

high temporal resolutions (Figures 4a–4c). The noise and sudden jumps observed in the single-system gradients are significantly reduced in the multi-GNSS solution, benefitting from the increased number of observed satellites and improved observation geometry.

Figure 5 shows the linear correlation between GPS (Figure 5, left), GLONASS (Figure 5, middle), and multi-GNSS (Figure 5, right) gradients versus the ECMWF gradients at station ONS1 for DOY 60–150 of 2014. Figures 5a–5e illustrate the gradients estimated with time resolutions of 1 h, 2 h, 4 h, 6 h, and 12 h. As shown in Figure 5a, the correlation coefficient between GPS and ECMWF gradients is 0.55, while the correlation coefficient between GLONASS and ECMWF gradients is about 0.46. We also calculate the correlation coefficient between the multi-GNSS gradients and the ECMWF gradients, which is about 0.65. Compared to GPS and GLONASS estimates, the correlation for the multi-GNSS processing is improved by about 18.2% and 41.3%, respectively. This improvement in the multi-GNSS processing can also be observed for the other resolutions (Figures 5b–5d). From the left panel of subfigures, which show the GPS solution, one can see that the 4 h gradients show the highest correlation with the ECMWF gradients probably due to the trade-off between increasing the temporal resolution and keeping sufficient redundancy of the parameters. As shown in Figure 5 (middle), GLONASS gradients present similar characteristics to GPS gradients; however, the correlation coefficients are slightly lower than in the GPS case. For the multi-GNSS solutions (Figure 5, right), the correlation coefficients are larger than for the single-system solutions. Here the 2 h multi-GNSS gradients achieve a highest correlation of 0.69, what demonstrates that with a higher observation density, sufficient redundancy of the parameters can be reached already with a 2 h resolution.

Table 1 summarizes the average values of the correlation coefficients between GNSS and ECMWF gradients at all four-system stations (shown in Figure 1) from

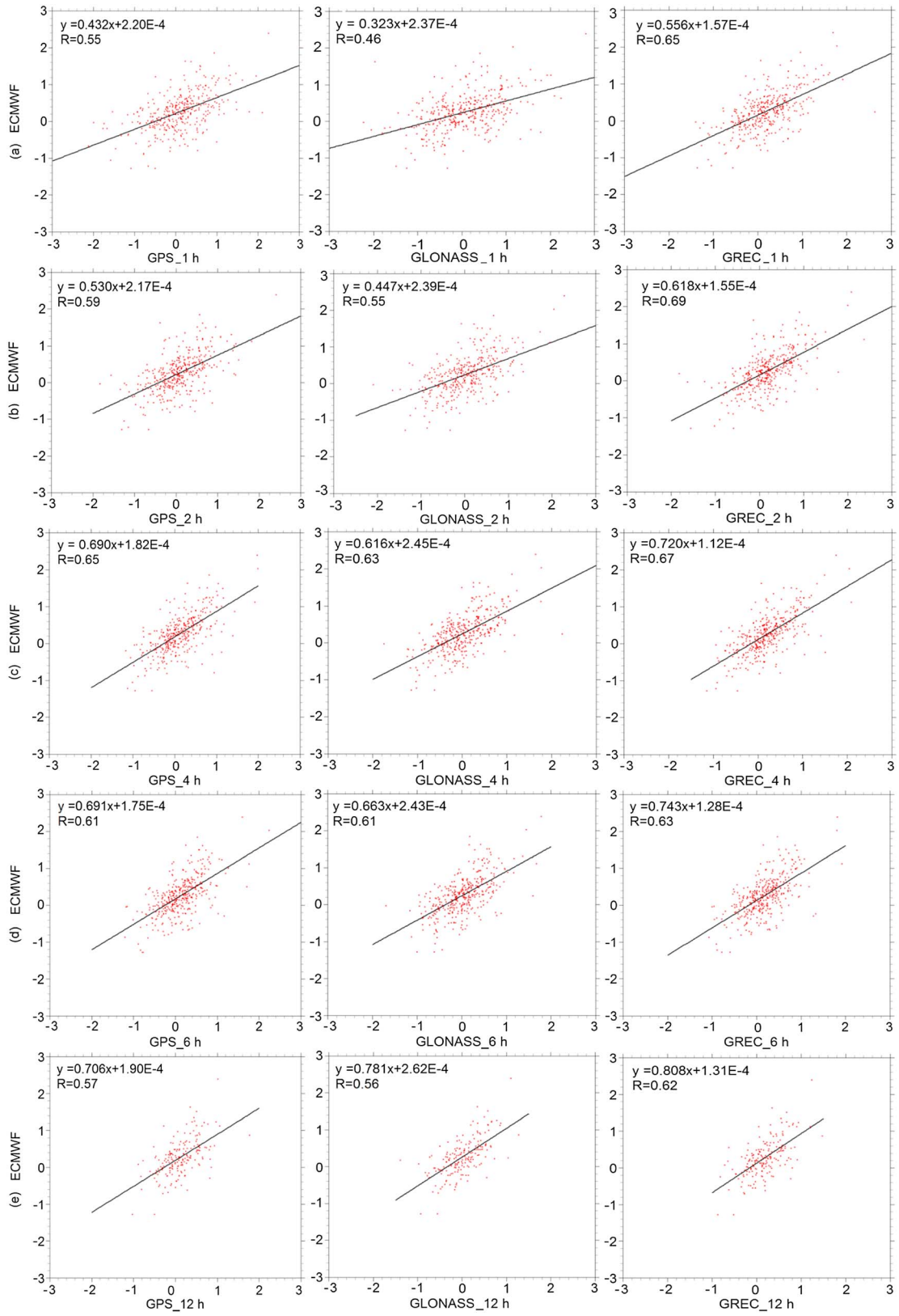

Figure 5. Correlation between the gradients from (left column) GPS, (middle column) GLONASS, and (right column) multi-GNSS solution versus the ECMWF gradients at station ONS1 for DOY 60–150 of 2014. (a–e) The gradients estimated for the temporal resolutions of 1 h, 2 h, 4 h, 6 h, and 12 h are illustrated. The vertical and horizontal axes show ECMWF and GNSS gradients (mm), respectively. The results of the linear regression and the correlation coefficients (*R*) are also shown.

Table 1. The Average Values of the Correlation Coefficients Between GPS, GLONASS, and Multi-GNSS Gradients Versus ECMWF Gradients at All Four-System Stations for Different Temporal Resolutions

Correlation With ECMWF	G	R	GREC
1 h	0.46	0.40	0.57
2 h	0.52	0.50	0.63
4 h	0.59	0.57	0.60
6 h	0.56	0.56	0.59
12 h	0.53	0.52	0.56

the MGEX network discerned by temporal resolutions. The correlation coefficient of the 2 h multi-GNSS gradients is largest at around 0.63. Compared to GPS and GLONASS estimates, the correlation coefficient in the multi-GNSS processing is improved by about 21.1% and 26.0%. These results confirm our findings for station ONS1 being valid for the majority of MGEX sites: high-resolution multi-GNSS gradients show better agreement with ECMWF gradients than low-resolution gradients, and more accurate and stable tropospheric gradients can be obtained from the multi-GNSS processing than from the single-system solutions.

3.2. Validation With WVR Gradients

To further validate the GNSS gradients, observations from the WVR co-located with the multi-GNSS station ONS1 are employed for the purpose of further external validation. The WVR gradients are calculated with a temporal resolution of 1 h as described in section 2.2. The GNSS gradients retrieved for different temporal resolutions (1 h, 2 h, 4 h, 6 h, and 12 h) for three months (DOY 60–150) during 2014 are shown in Figure 6. The WVR gradients are also depicted in blue lines in the same figure for comparison. Figure 6a displays GPS gradients estimated with the temporal resolutions of 1 h, 2 h, and 4 h in Figure 6 (left column), and time

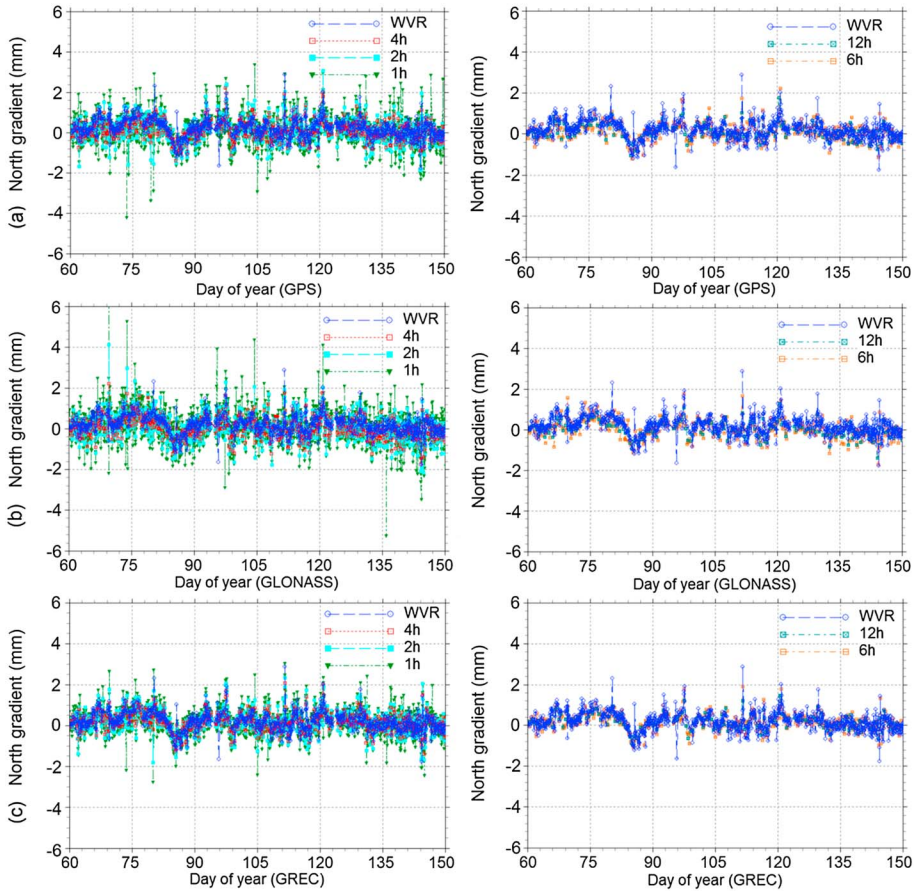

Figure 6. The gradients estimated with different temporal resolutions at station ONS1 for DOY 60–150 of 2014. (a) GPS, (b) GLONASS, and (c) multi-GNSS gradients are illustrated. The gradients of 1 h, 2 h, and 4 h are shown in the left column, while those estimated every 6 h and 12 h are shown in the right column. The blue lines show the tropospheric gradients derived from WVR.

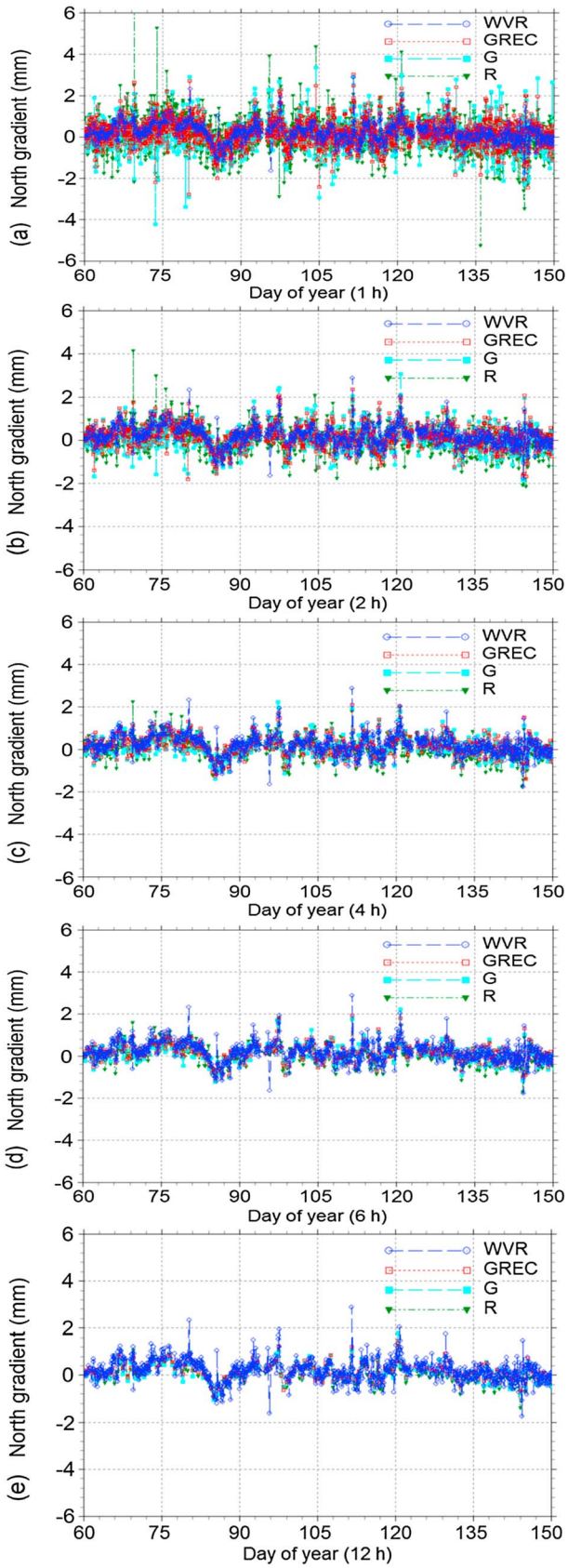

resolutions of 6 h and 12 h in Figure 6 (right column). Also here, it can be seen that the 1 h GPS gradients exhibit the largest noise, resulting from short session spans and limited observation geometry. In contrast, although the 6 h and 12 h estimates contain much less noise, however, some peaks are not captured by GNSS gradients due to the longer time interval. The best agreement with the WVR gradients can be observed for the 2 h and 4 h gradients, where not only is less noise present, but also, most of the spike-shaped peaks of the gradients are well captured. GLONASS gradients show similar features to the GPS gradients (Figure 6b), although they are slightly noisier than GPS gradients. However, concerning the multi-GNSS gradients (Figure 6c), one can see that the noise in the high-resolution estimates is significantly reduced. Here the 1 h estimates show better agreement with the WVR gradients than the 2 h and 4 h estimates in terms of capturing the peaks, which is slightly different from the results when comparing with ECMWF gradients, where the 2 h resolutions performed the best. Nevertheless, both validations proof that the geometrical defects of high-resolved gradients can be limited considering multi-GNSS processing. Possible reasons could include the fact that the ECMWF gradients are model values sampled every 6 h and on a $1° \times 1°$ grid, which is smoother; also, while the WVR gradients are in situ observations which directly record the actual atmospheric gradients at the site with a very high temporal resolution. Considering the results of both validations (ECMWF and WVR), we demonstrate that the temporal resolution of atmospheric gradients investigated in this study can be as high as 1 h.

Figure 7. The gradients derived from GPS, GLONASS, and the multi-GNSS solutions at station ONS1 for DOY 60–150 of 2014. The gradients estimated with time resolutions of (a) 1 h, (b) 2 h, (c) 4 h, (d) 6 h, and (e) 12 h. The blue lines indicate the tropospheric gradients derived from WVR.

Figure 7 shows the gradients derived from GPS, GLONASS, and multi-GNSS solutions at station ONS1 for the same period. Figures 7a–7e show the gradients estimated with the time resolutions of 1 h, 2 h, 4 h, 6 h, and 12 h, respectively. The WVR gradients are depicted in blue lines. It can be seen from Figure 7 that a good agreement with the WVR gradients can be observed for GPS gradients in general. GLONASS gradients reveal comparable results to GPS, but with slightly more noise. Compared to the single-system solutions, the multi-GNSS gradients are much more stable and present the best agreement with the WVR gradients. The noise found in the single-system solutions is significantly reduced in the combined solution, especially in the case of the high resolutions.

Figure 8 shows the linear correlation between GPS (Figure 8, left column), GLONASS (Figure 8, middle column), and multi-GNSS (Figure 8, right column) gradients with respect to the WVR gradients. Figures 8a–8e illustrate the gradients estimated with the time resolutions of 1 h, 2 h, 4 h, 6 h, and 12 h, respectively. As shown in Figure 8a, the correlation coefficient between GPS and WVR gradients is about 0.52, and the correlation between GLONASS and WVR is 0.46. We also calculate the correlation coefficient between the multi-GNSS and the WVR gradients, which is about 0.64. Compared to GPS and GLONASS estimates, the correlation for the combined solution with respect to the individual single-system solution is improved by about 23.1% and 39.1%, respectively. The estimates retrieved with the other resolutions (Figures 8b–8e) show similar improvements through the multi-GNSS processing. The improvement percentage is reduced when the estimation time interval increases. Moreover, one can see from Figure 8 (right column) that the high-resolution multi-GNSS gradients show higher correlation with the WVR gradients than the low-resolution gradients. The 1 h multi-GNSS gradients display the highest correlation of 0.64, while the single-system estimates (GPS in Figure 8 (left column) and GLONASS in Figure 8 (middle column)) do not show significant improvement due to the high temporal resolution. The validation using WVR data further confirms the aforementioned conclusions related to the benefit of multi-GNSS processing, as well as the benefit of high temporal resolution for tropospheric gradient retrieval. Therefore, we conclude that accurate and stable tropospheric gradient estimates with high temporal resolution (up to 1 h) can be achieved with the multi-GNSS fusion. These demonstrate the significant potential contribution of multi-constellation GNSS in the reconstruction of atmospheric water vapor, as well as for meteorological applications such as numerical weather prediction and nowcasting.

3.3. Comparison of Co-located GNSS Stations

In order to evaluate the internal consistency of GNSS gradients and the performance of high-precision multi-GNSS gradients, data from co-located GNSS stations are investigated. Figure 9 shows the north gradients derived from GPS, GLONASS, and the multi-GNSS solution at co-located GNSS stations KOUG/KOUR operated at Kourou, French Guiana, for DOY 60–150 of 2014. Figure 9a shows the gradient estimates derived from the multi-GNSS processing with temporal resolutions of 2 h, 4 h, and 12 h. Although the 2 h and 4 h gradients show some noise, it can be seen that they show very good agreement. Good agreement can also be found for the 12 h resolution, which shows the low sampling rate of the gradient estimates.

Figure 9b gives the linear correlation of GPS gradients estimated with temporal resolutions of 2 h (left), 4 h (middle), and 12 h (right) at the two stations. One can see that the GPS gradients at the two stations show high correlation, which indicates the good internal consistency of gradient estimates from GPS. Besides, the gradients estimated every 12 h reveal a highest correlation of 0.72. When the gradients are estimated every 12 h instead of high resolution (e.g., 2 h), some peaks in the gradient estimates disappear for both stations, resulting in the highly correlated estimates. However, the low-resolution gradients cannot well represent the temporal variation of the actual tropospheric gradients; thus they are not recommended for precise meteorological applications. Similar results are observed for the GLONASS and multi-GNSS estimates (Figures 9c and 9d). As shown in the three panels of the subfigures, we can notice that GLONASS gradients are slightly worse than GPS estimates, and the correlation between the two stations obviously increases by the multi-GNSS processing compared to the single-system solutions. The higher the temporal resolution is, the more the correlation improves. These high correlations demonstrate the good internal consistency of high-resolution GNSS gradient estimates, especially for the multi-GNSS processing.

4. Effects on Precise Positioning

4.1. Repeatability of Station Position Estimates

As another main topic of our study, the influence of modeling the tropospheric gradients on station position estimates is discussed in this section. We first investigate the effects of gradient estimates on static precise

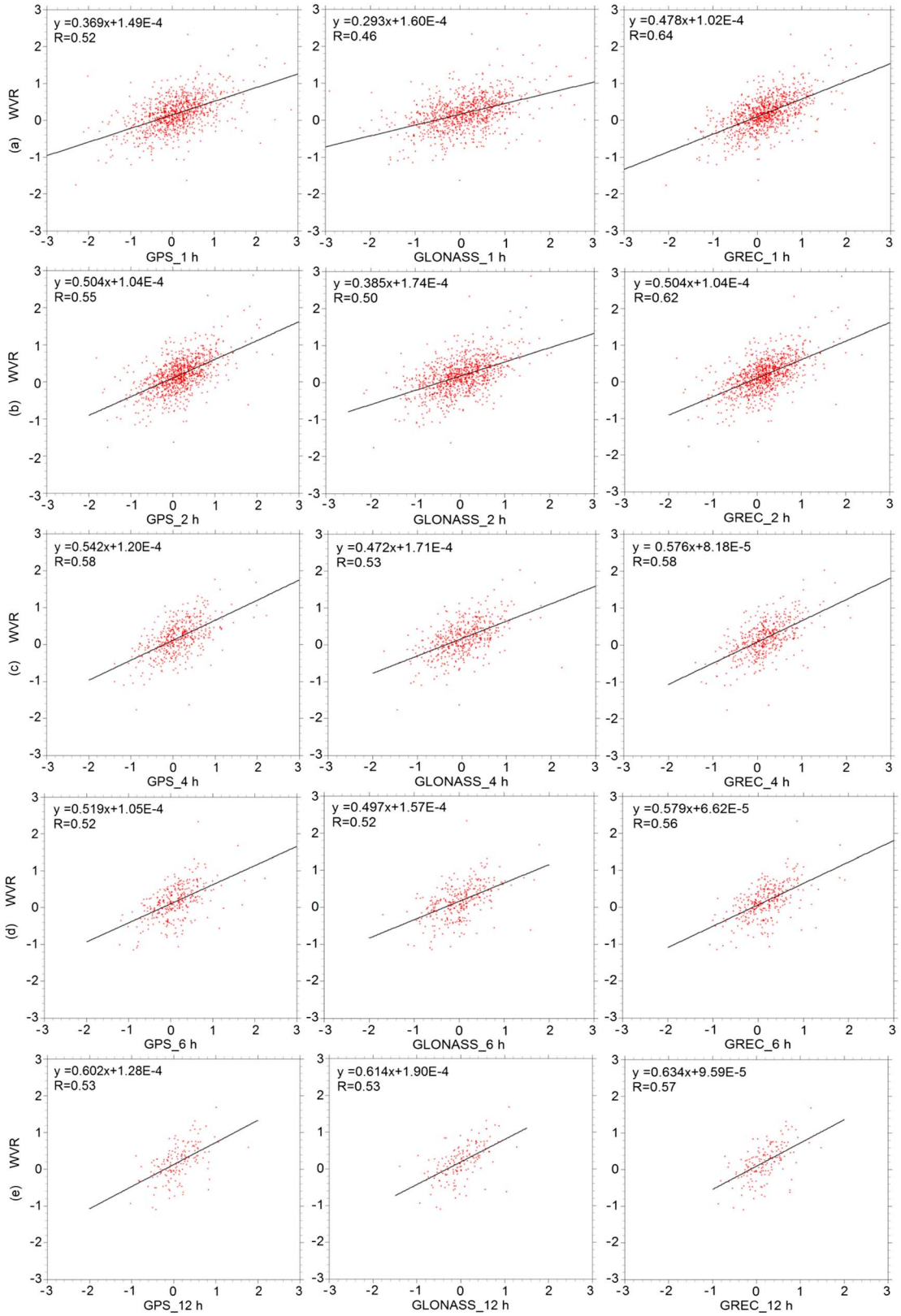

Figure 8. Correlation between the gradients from (left column) GPS, (middle column) GLONASS, and the (right column) multi-GNSS solution with respect to the WVR gradients at station ONS1 for DOY 60–150 of 2014. The gradients estimated with the time resolutions of (e) 1 h, (b) 2 h, (c) 4 h, (d) 6 h, and (e) 12 h are illustrated. The vertical and horizontal axes show WVR and GNSS gradients (mm), respectively. The results of the linear regression and the correlation coefficients (R) are also given.

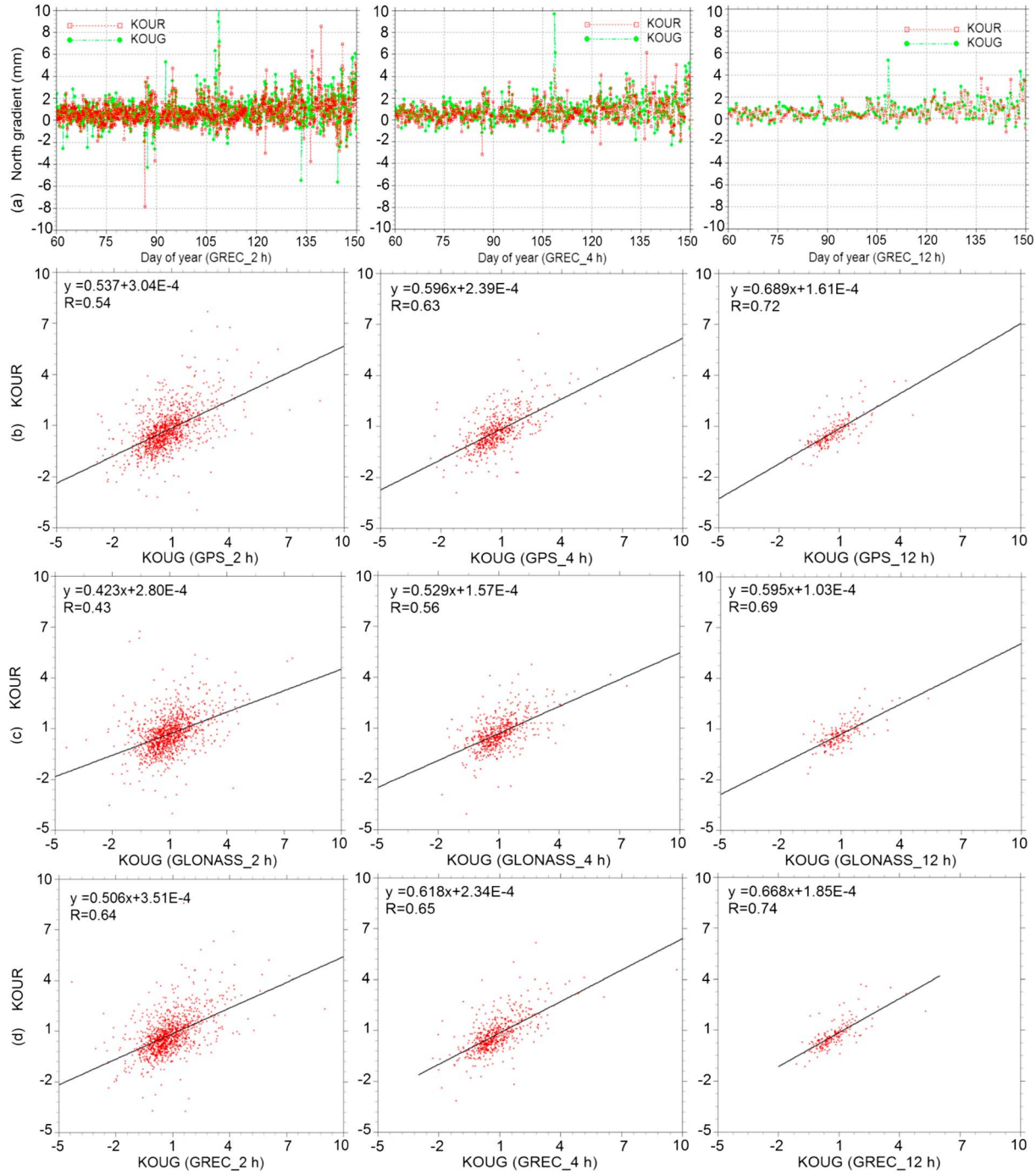

Figure 9. The gradients derived from GPS, GLONASS and multi-GNSS solutions for different temporal resolutions of 2 h (left), 4 h (middle), and 12 h (right) at co-located stations KOUG/KOUR for DOY 60–150 of 2014. (a) The gradients derived from the multi-GNSS processing. (b) The linear correlation of GPS gradients. (c) The linear correlation of GLONASS gradients. (d) The linear correlation of the multi-GNSS gradients.

positioning. We calculate the repeatability of station coordinate estimates from daily PPP processing when gradients are estimated with different temporal resolutions, and with the single-system and multi-GNSS data. Figure 10 shows the repeatability (standard deviations, STD) of the station coordinates (north, east, and up) derived from GPS, GLONASS, and multi-GNSS with different temporal resolutions for ten stations during DOY 60–150 of 2014. Figures 10a–10c illustrate GPS, GLONASS, and multi-GNSS solution, where the results for the north, east, and up components are displayed in the left, middle, and right plots, respectively.

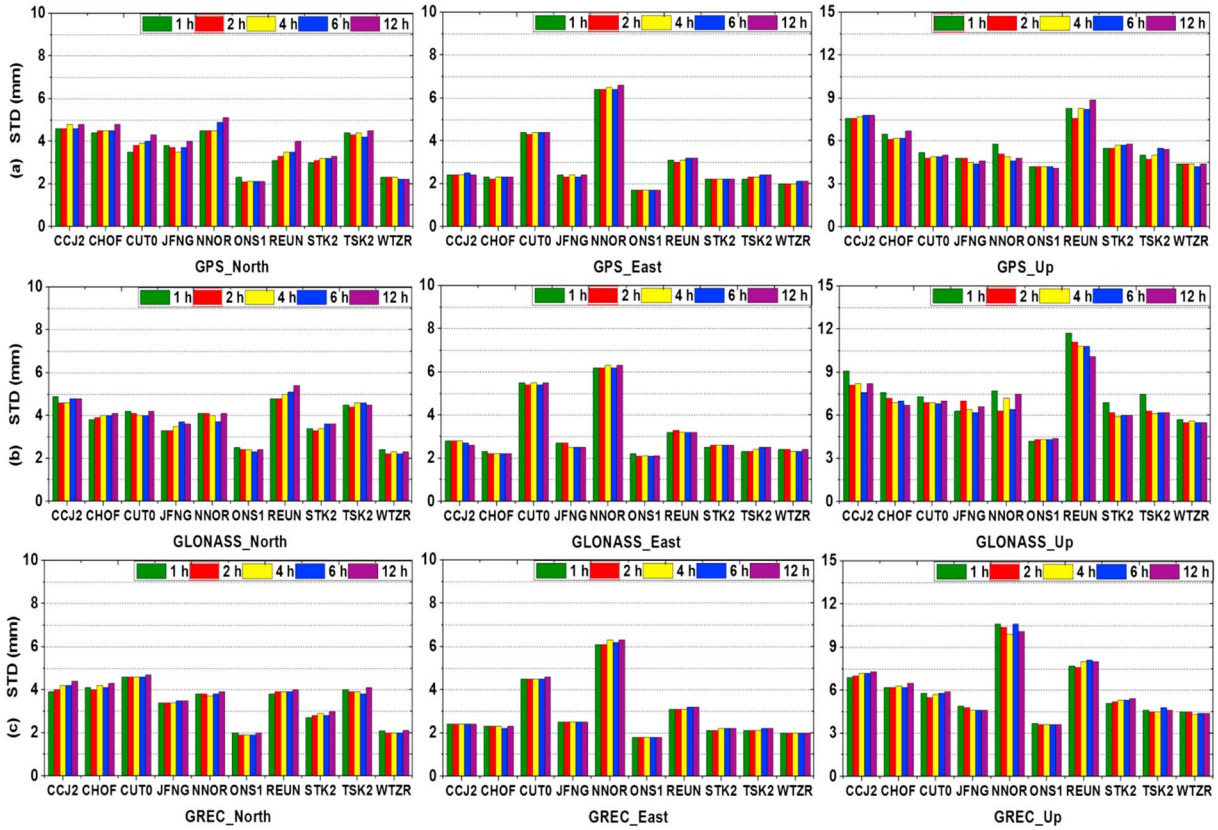

Figure 10. The repeatability of station coordinates derived from GPS, GLONASS, and multi-GNSS daily PPP solutions for ten stations for DOY 60–150 of 2014. The results for (a) GPS, (b) GLONASS, and (c) multi-GNSS solutions are shown. Different temporal resolutions of 1 h, 2 h, 4 h, 6 h, and 12 h are depicted in different colors. The north, east, and up components are shown in the left, middle, and right plots, respectively.

We can see from Figure 10a that, in general, the repeatability of the station coordinates is at the level of a few millimeters for the GPS solution. The station position repeatability for most of the stations is improved when the gradients are estimated with high temporal resolutions (e.g., 4 h) compared to the commonly used low-resolution gradient (e.g., 12 h) estimation strategy. This is especially the case for the north component, where the average repeatability is about 3.8 mm for the high-resolution estimates and about 4.3 mm for the low-resolution estimates, an improvement of about 13.2%. The average improvement of station position repeatability is about 11.1% and 8.3% for the east and up components, respectively. Only at a few stations (e.g., WTZR and ONS1), an improvement in the high-resolution gradient estimation cannot be clearly observed. A similar phenomenon and comparable results can be found for the GLONASS solution (Figure 10b), where the improvement of repeatability, comparing high-resolution estimates to low-resolution estimates, is about 13.0%, 10.6%, and 8.0% for the north, east, and up components, respectively. For the multi-GNSS solutions (Figure 10c), the improvement in the repeatability of station coordinates benefitting from the high-resolution gradient estimates is clearly observed for almost all stations, although the magnitude of the improvement is sometimes less significant, at around 8.3%, 8.0%, and 8.3% for the north, east, and up components.

To enhance knowledge in relation to the comparison between the single-system and the combined solutions, Figure 11 shows the station coordinate repeatability for the north component for GPS, GLONSSS, and multi-GNSS solutions when the tropospheric gradients are estimated with different temporal resolutions (1 h, 2 h, 4 h, 6 h, and 12 h). One can see that the station coordinate repeatability for GLONASS is slightly worse than for GPS, while the best results are found in the multi-GNSS solutions in comparison to the two single-system solutions in both high-resolution and low-resolution gradient estimation modes. Taking the 4 h gradient estimation as an example, the station coordinate repeatability is about 2.3–4.9 mm for GPS, 2.4–5.0 mm for GLONASS, and 2.0–4.4 mm for the multi-GNSS. When the gradients are estimated with a low temporal resolution (e.g., 12 h), the station repeatability is about 2.2–5.1 mm for GPS, 2.4–5.1 mm for GLONASS, and 2.1–4.7 mm

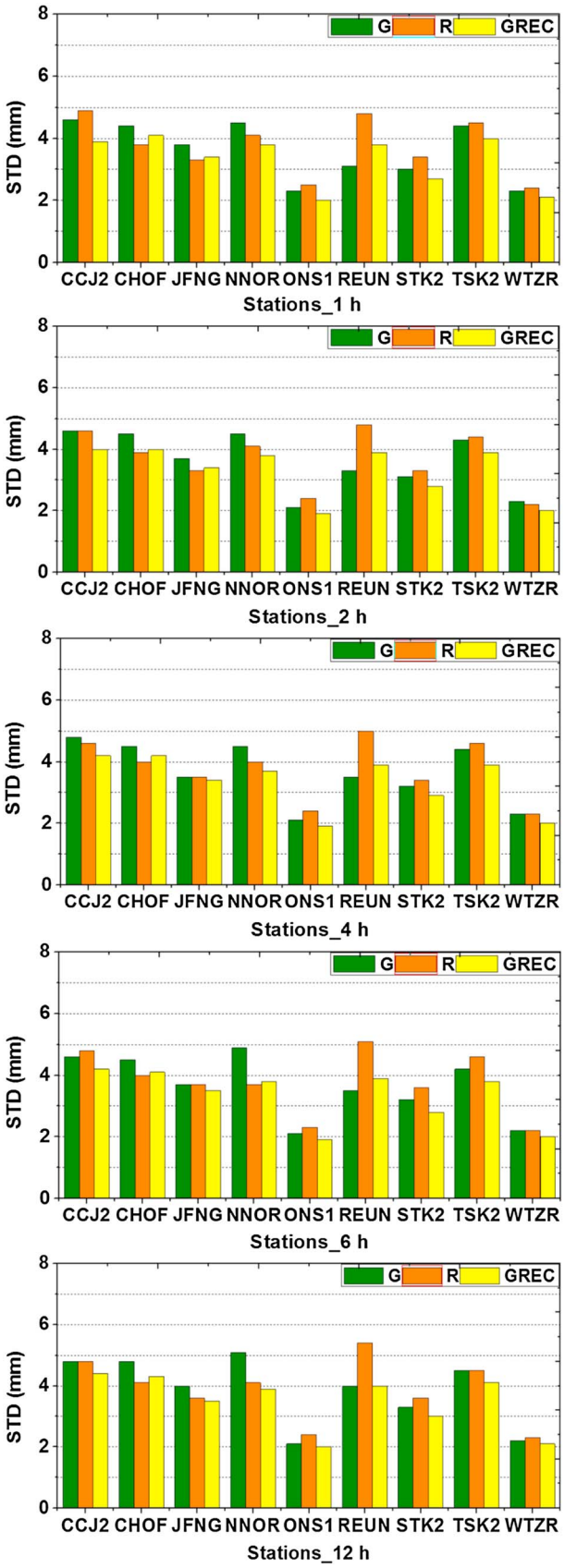

Figure 11. Comparison of station coordinate repeatability for different temporal resolutions (1 h, 2 h, 4 h, 6 h, and 12 h). GPS, GLONSSS, and multi-GNSS estimates are displayed in olive, orange, and yellow colors, respectively.

for the multi-GNSS solutions. Based on these results, we conclude that station coordinate repeatability can be clearly improved by a multi-GNSS fusion, and better results can be achieved if the high-resolution gradient estimation instead of the commonly used daily gradient estimation is performed, especially in the multi-GNSS data processing.

Although the gradients derived from BeiDou are presently not sufficiently accurate, as pointed out in section 3.1, it is nevertheless still worth investigating the effect of tropospheric gradient estimation on BeiDou precise positioning. Figure 12 shows the station coordinate repeatability of BeiDou daily PPP solutions when the gradients are estimated every 2 h, 4 h, and 12 h at stations GMSD, JFNG, and NNOR for DOY 60–150 of 2014. The results for the north, east, and up components are given in the left, middle, and right plots, respectively. As shown in Figure 12, the station coordinate repeatability of BeiDou PPP is at the millimeter level for the horizontal components and centimeter level for the up component. In comparison to the previous results for GPS, GLONASS, and multi-GNSS solutions, the accuracy of BeiDou PPP is significantly worse. Meanwhile, better station coordinate repeatability can be achieved for BeiDou when the gradients are estimated with low temporal resolutions. Compared to high-resolution gradient estimation, repeatability is improved by about 10.3%, 4.5%, and 9.8% for the north, east, and up components in case of the low-resolution gradient estimation. This might be attributable to worse observation geometry, the signal instability, and the lower precision of the correction models for BeiDou (e.g., the PCO and PCV models). Thus, estimating the tropospheric gradients with a

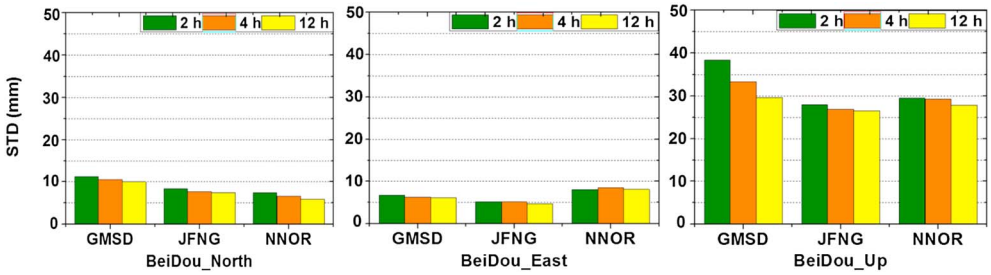

Figure 12. The station coordinate repeatability of BeiDou daily PPP solutions when the gradients are estimated every 2 h, 4 h, and 12 h at stations GMSD, JFNG, and NNOR for DOY 60–150 of 2014. The results for the north, east, and up components are shown in the left, middle, and right plots, respectively.

low temporal resolution (e.g., on a daily basis) for the current BeiDou constellation will enhance the solution strength and reduce the errors, rather than the high-resolution gradients that work well for the developed satellite systems (e.g., GPS) and the multi-GNSS fusion.

4.2. Effects of Gradient Estimation on Kinematic PPP

The effect of tropospheric gradient estimation on kinematic precise positioning is investigated in this section. Here all stations are processed in simulated kinematic mode (the station coordinates are estimated epoch by epoch). Table 2 summarizes the results for STD of GPS and multi-GNSS kinematic PPP when the gradients are estimated with the temporal resolutions of 2 h, 4 h, and 12 h at station ONS1 for DOY 097 of 2014. For both GPS and multi-GNSS kinematic positioning, the STD values get smaller when the gradients are estimated with higher temporal resolution, compared to the low-resolution gradient estimation. The STD values for the north, east, and up components are reduced by about 18.7%, 3.9%, and 2.3% for GPS, and 10.9%, 7.0%, and 3.4% for multi-GNSS processing. Moreover, comparing the multi-GNSS with GPS solutions, the precision of station positions is clearly improved. The improvements for the north, east, and up components are about 8.2%, 18.4%, and 6.7% for high-resolution gradient estimation, and 12%, 15.7%, and 5.6% for low-resolution gradient estimations. These results are similar to those for the static PPP and further confirm the aforementioned findings related to the benefit of high-resolution tropospheric estimations as well as the multi-GNSS fusion on precise positioning.

5. Conclusions

In this contribution, we develop a multi-GNSS (Global Navigation Satellite Systems) process with high-resolution tropospheric delay gradient estimation. Observation data from the IGS (International GNSS Service) MGEX (Multi-GNSS Experiment) network are analyzed, and the tropospheric delay gradients with different temporal resolutions retrieved from both single-system and multi-GNSS solutions are validated with NWM (numerical weather models) and WVR (water vapor radiometer) data. The results demonstrate that GLONASS gradients achieve comparable accuracy to GPS gradients, but exhibit slightly more noise and outliers. The multi-GNSS gradients behave with much greater stability than the single-system estimates, especially in cases of high temporal resolutions, benefitting from the increased number of observed satellites and improved observation geometry. The correlation coefficient between 2 h multi-GNSS gradients and ECMWF (European Centre for Medium-Range Weather Forecasts) gradients is the largest at around 0.63. Compared to GPS and GLONASS estimates, the correlation for the multi-GNSS processing is improved by about 21.1% and 26.0%. These results indicate that high-resolution multi-GNSS gradients agree better with the ECMWF gradients than the low-resolution gradients; in addition, more accurate and stable tropospheric gradients can be obtained from the multi-GNSS processing than from the single-system processing.

Table 2. The STD of GPS and Multi-GNSS Kinematic PPP for Different Temporal Resolutions (2 h, 4 h, and 12 h) at Station ONS1

	2 h			4 h			12 h		
STD	N	E	U	N	E	U	N	E	U
GPS	6.1	9.7	21.2	6.1	9.9	20.9	7.5	10.2	21.6
GREC	5.5	8.1	19.9	5.8	7.8	19.4	6.4	8.6	20.4

Compared to GPS and GLONASS gradients, the multi-GNSS estimates present the best agreement with WVR gradients and the correlation coefficient for the combined solution is improved by about 23.1% and 39.1%, respectively. The high-resolution multi-GNSS gradients show higher correlation with the WVR gradients than the low-resolution gradients. Validation with WVR data further confirms aforementioned conclusions related to the benefit of multi-GNSS processing, as well as the benefit of high temporal resolutions for tropospheric gradient retrieving. Our findings demonstrate the significant potential contribution of multi-constellation GNSS in terms of reconstructing the atmospheric water vapor, as well as to meteorological applications such as numerical weather prediction and nowcasting.

The effects of high-resolution gradient estimation on precise positioning in both static and kinematic modes are also investigated. The station coordinate repeatability for GLONASS is slightly worse than for GPS, while the multi-GNSS solutions present the best repeatability in comparison with the two single-system solutions in both high-resolution and low-resolution gradient estimation modes. For the multi-GNSS solutions, the improvement in repeatability of station coordinates benefitting from the high-resolution gradient estimates is also clearly observed at almost all stations. We can conclude that the station coordinate repeatability can be clearly improved by multi-GNSS fusion, and better results can be achieved if the high-resolution gradient estimation instead of the commonly used daily gradient estimation is applied, especially during multi-GNSS data processing.

For both GPS and multi-GNSS kinematic positioning, the STD (standard deviation) values get smaller when the gradients are estimated with higher temporal resolution. Moreover, comparing the multi-GNSS with GPS solutions, the precision of station positions is clearly improved; improvements for the north, east, and up components are about 8.2%, 18.4%, and 6.7% for high-resolution gradient estimation and 12%, 15.7%, and 5.6% for the low-resolution gradient estimation. These results confirm the benefit of multi-GNSS processing as well as high-resolution tropospheric gradient estimation on precise positioning. Future studies will focus on the data assimilation of the high-resolution multi-GNSS tropospheric gradient products into NWM for short-term forecasts and nowcasting of strong rainfall events.

Acknowledgments
Many thanks go to the International GNSS Service (IGS) for providing multi-GNSS data available at ftp://cddis.gsfc.nasa.gov/gnss/data/campaign/mgex/. We also thank the ECMWF for the online provision of the model data of meteorological information. Sincere thanks go to Gunnar Elgered and Peter Forkman for providing the WVR data from the Onsala Geodetic Observatory. One of the authors (C. Lu) is sponsored by the China Scholarship Council, which is gratefully acknowledged.

References

Bar-Sever, Y. E., P. M. Kroger, and J. A. Borjesson (1998), Estimating horizontal gradients of tropospheric path delay with a single GPS receiver, *J. Geophys. Res.*, *103*(B3), 5019–5035, doi:10.1029/97JB03534.

Bevis, M., S. Businger, T. Herring, C. Rocken, R. Anthes, and R. Ware (1992), GPS meteorology: Remote sensing of atmospheric water vapor using GPS, *J. Geophys. Res.*, *97*, 15,787–15,801.

Bevis, M., S. Businger, T. Chiswell, A. Herring, R. Anthes, C. Rocken, and R. Ware (1994), GPS meteorology: Mapping zenith wet delays onto precipitable water, *J. Appl. Meteorol.*, *33*, 379–386.

Böhm, J., A. Niell, P. Tregoning, and H. Schuh (2006), Global Mapping Function (GMF): A new empirical mapping function based on numerical weather model data, *Geophys. Res. Lett.*, *33*, L07304, doi:10.1029/2005GL025546.

Chen, G., and T. A. Herring (1997), Effects of atmospheric azimuth asymmetry on the analysis of space geodetic data, *J. Geophys. Res.*, *102*(B9), 20,489–20,502, doi:10.1029/97JB01739.

Dousa, J., and P. Vaclavovic (2014), Real-time zenith tropospheric delays in support of numerical weather prediction applications, *Adv. Space Res.*, *53*(9), 1347–1358.

Duan, J., et al. (1996), GPS meteorology: Direct estimation of the absolute value of precipitable water, *J. Appl. Meteorol.*, *35*, 830–838.

Elgered, G., and P. O. J. Jarlemark (1998), Ground-based microwave radiometry and long-term observations of atmospheric water vapor, *Radio Sci.*, *33*(3), 707–717, doi:10.1029/98RS00488.

Elgered, G., H. Plag, H. van der Marel, S. Barlag, and J. Nash (Eds.) (2005), COST 716: Exploitation of ground-based GPS for climate and numerical weather prediction applications, Final Report, European Community, EUR 21639, ISBN 92-898-0012-7.

Fang, P., M. Bevis, Y. Bock, S. Gutman, and D. Wolfe (1998), GPS meteorology: Reducing systematic errors in geodetic estimates for zenith delay, *Geophys. Res. Lett.*, *25*, 3583–3586.

Gendt, G., G. Dick, C. Reigber, M. Tomassini, Y. Liu, and M. Ramatschi (2004), Near real time GPS water vapor monitoring for numerical weather prediction in Germany, *J. Meteorol. Soc. Jpn.*, *82*, 361–370.

Ghoddousi-Fard, R., P. Dare, and R. Langley (2009), Tropospheric delay gradients from numerical weather prediction models: Effects on GPS estimated parameters, *GPS Solut.*, *13*(4), 281–291.

Gradinarsky, L., J. Johansson, H. Bouma, H. Scherneck, and G. Elgered (2002), Climate monitoring using GPS, *Phys. Chem. Earth*, *27*(4–5), 335–340, doi:10.1016/S1474-7065(02)00009-8.

Iwabuchi, T., S. Miyazaki, K. Heki, I. Naito, and Y. Hatanaka (2003), An impact of estimating tropospheric delay gradients on tropospheric delay estimations in the summer using the Japanese nationwide GPS array, *J. Geophys. Res.*, *108*(D10), 4315, doi:10.1029/2002JD002214.

Karabatic, A., R. Weber, and T. Haiden (2011), Near real-time estimation of tropospheric water vapour content from ground based GNSS data and its potential contribution to weather now-casting in Austria, *Adv. Space Res.*, *47*, 1691–1703.

Kouba, J. (2009), A Guide to Using International GNSS Service (IGS) Products. [Available at http://igscb.jpl.nasa.gov/igscb/resource/pubs/UsingIGSProductsVer21.pdf.]

Li, X., G. Dick, M. Ge, S. Heise, J. Wickert, and M. Bender (2014), Real-time GPS sensing of atmospheric water vapor: Precise point positioning with orbit, clock and phase delay corrections, *Geophys. Res. Lett.*, *41*, 3615–3621, doi:10.1002/2013GL058721.

Li, X., F. Zus, C. Lu, G. Dick, T. Ning, M. Ge, J. Wickert, and H. Schuh (2015a), Retrieving of atmospheric parameters from multi-GNSS in real time: Validation with water vapor radiometer and numerical weather model, *J. Geophys. Res. Atmos.*, *120*, 7189–7204, doi:10.1002/2015JD023454.

Li, X., M. Ge, X. Dai, X. Ren, M. Fritsche, J. Wickert, and H. Schuh (2015b), Accuracy and reliability of multi-GNSS real-time precise positioning: GPS, GLONASS, BeiDou, and Galileo, *J. Geod.*, *89*(6), 607–635.

Li, X., X. Zhang, X. Ren, M. Fritsche, J. Wickert, and H. Schuh (2015c), Precise positioning with current multi-constellation Global Navigation Satellite Systems: GPS, GLONASS, Galileo and BeiDou, *Sci. Rep.*, *5*, 8328, doi:10.1038/srep08328.

Li, X., F. Zus, C. Lu, T. Ning, G. Dick, M. Ge, J. Wickert, and H. Schuh (2015d), Retrieving high-resolution tropospheric gradients from multi-constellation GNSS observations, *Geophys. Res. Lett.*, *42*, 4173–4181, doi:10.1002/2015GL063856.

Li, Z., J.-P. Muller, and P. Cross (2003), Comparison of precipitable water vapor derived from radiosonde, GPS, and Moderate-Resolution Imaging Spectroradiometer measurements, *J. Geophys. Res.*, *108*(D20), 4651, doi:10.1029/2003JD003372.

MacMillan, D. (1995), Atmospheric gradients from very long baseline interferometry observations, *Geophys. Res. Lett.*, *22*(9), 1041–1044, doi:10.1029/95GL00887.

Meindl, M., S. Schaer, U. Hugentobler, and G. Beutler (2004), Tropospheric gradient estimation at CODE: Results from Global Solutions, *J. Meteorol. Soc. Jpn.*, *82*, 331–338, doi:10.2151/jmsj.2004.331.

Miyazaki, S., T. Iwabuchi, K. Heki, and I. Naito (2003), An impact of estimating tropospheric delay gradients on precise positioning in the summer using the Japanese nationwide GPS array, *J. Geophys. Res.*, *108*(B7), 2335, doi:10.1029/2000JB000113.

Montenbruck, O., P. Steigenberger, R. Khachikyan, G. Weber, R. B. Langley, L. Mervart, and U. Hugentobler (2014), IGS-MGEX: Preparing the ground for multi-constellation GNSS science, *Inside GNSS*, *9*(1), 42–49.

Nilsson, T., and G. Elgered (2008), Long-term trends in the atmospheric water vapor content estimated from ground-based GPS data, *J. Geophys. Res.*, *113*, D19101, doi:10.1029/2008JD010110.

Poli, P., P. Moll, F. Rabier, G. Desroziers, B. Chapnik, L. Berre, S. B. Healy, E. Andersson, and F.-Z. El Guelai (2007), Forecast impact studies of zenith total delay data from European near real-time GPS stations in Météo France 4DVAR, *J. Geophys. Res.*, *112*, D06114, doi:10.1029/2006JD007430.

Rocken, C., T. Van Hove, and R. Ware (1997), Near real-time sensing of atmospheric water vapor, *Geophys. Res. Lett.*, *24*, 3221–3224.

Saastamoinen, J. (1973), Contributions to the theory of atmospheric refraction - Part II. Refraction corrections in satellite geodesy, *Bull. Géod.*, *47*(1), 13–34, doi:10.1007/BF02522083.

Shoji, Y. (2013), Retrieval of water vapor inhomogeneity using the Japanese nationwide GPS array and its potential for prediction of convective precipitation, *J. Meteorol. Soc. Jpn.*, *91*, 43–62.

Zumberge, J. F., M. B. Heflin, D. C. Jefferson, M. M. Watkins, and F. H. Webb (1997), Precise point positioning for the efficient and robust analysis of GPS data from large networks, *J. Geophys. Res.*, *102*(B3), 5005–5017.

Zus, F., G. Dick, J. Dousa, S. Heise, and J. Wickert (2014), The rapid and precise computation of GPS slant total delays and mapping factors utilizing a numerical weather model, *Radio Sci.*, *49*, 207–216, doi:10.1002/2013RS005280.